# Modeling of Viscous Fingering

Ekkehard Holzbecher
Georg-August Universität Göttingen
GZG, Goldschmidtstr. 3, 37077 Göttingen, GERMANY
E-Mail: eholzbe@gwdg.de

**Abstract:** Viscous fingering is a topic of interest since the beginning of computational fluid dynamics. Here we focus on the classical constellation of miscible displacement, as it has been investigated in Hele-Shaw cells. A temperature or salinity front is entering with a fluid that has a different viscosity. The pure 1D flow is destabilized by the Saffman-Taylor instability. Using COMSOL Multiphysics we investigate the solution of a 2D generic set-up in an Eulerian system. Initial conditions near the inlet are described by a random function. We explore the fingering solutions in terms of various numerical parameters, i.e. for meshes of various type and refinement. For various solvers we examine the execution time, i.e. the performance of the model.

**Keywords:** viscous fingering, streamfunction, streamlines.

## 1. Introduction

Fingering phenomena can observed in several fields of application, especially in porous media flow. It is relevant in oil and gas reservoirs, esp. for water oil displacement [i]. It is also relevant concerning $CO_2$ sequestration into deep aquifers (Garcia & Pruess [ii]). Fingering is observed at contaminated groundwater sites, where non-aqueous phase liquids penetrate the aquifer (Zhang & Smith [iii]). Perugini *et al.* [iv] find evidence for viscous fingering in magmatic structures of Antarctica. Zitha *et al.* [v] study viscous fingering in a foam drainage problem.

Here we focus on the classical constellation of miscible displacement, as it has been investigated in Hele-Shaw cells, i.e. laboratory set-ups for 2D flow of a highly viscous fluid. Under usual conditions the analytical description is the same for Hele-Shaw cells and porous media flow. In the test-case a temperature or salinity front is entering with a fluid which is characterized by a drastically changing viscosity. The system is destabilized by the Saffman-Taylor instability [vi].

## 2. Governing Equations

As Zimmerman & Homsy [vii] we start with the system:

$$\nabla \bullet \mathbf{u} = 0 \qquad \mathbf{u} = -\frac{\mathbf{k}}{\mu}\nabla p \tag{1}$$

$$\varphi \frac{\partial c}{\partial t} = \nabla \bullet \left(\mathbf{D}\nabla\right) c - \mathbf{u} \bullet \nabla c \tag{2}$$

which is valid in the Eulerian coordinate system. The first equation expresses the conservation of fluid mass in terms of the velocity vector **u**. It is valid for incompressible fluids. In porous media flow **u** denotes the Darcy-velocity. The second equation is Darcy's Law for porous media flow, where **k** denotes the permeability tensor, $\mu$ kinematic viscosity and $p$ dynamic pressure. Note here already that viscosity is a variable. For free fluids in Hele-Shaw cells the given description holds, if the permeability is set to $k = d^2/12$, where $d$ denotes the space between the two plates of the cell. The third equation is the transport equation, describing the distribution of a component in space and time. The independent variable is the concentration $c$. $\varphi$ denotes the porosity, which has to be set to unity for flow in Hele-Shaw cells. **D** is the dispersion tensor, which in 2D is given by:

$$\mathbf{D} = \begin{pmatrix} \left(\alpha_L u_x^2 + \alpha_T u_y^2\right)/|\mathbf{u}| & \left(\alpha_L - \alpha_T\right) u_x u_y / |\mathbf{u}| \\ \left(\alpha_L - \alpha_T\right) u_x u_y / |\mathbf{u}| & \left(\alpha_L u_y^2 + \alpha_T u_x^2\right)/|\mathbf{u}| \end{pmatrix} \tag{3}$$

where $\alpha_L$ denotes the dispersivity in longitudinal direction and $\alpha_T$ the dispersivity in transversal direction. $u_x$ and $u_y$ are the components of the velocity vector **u**. Molecular diffusivity is not used in this model. The dispersion tensor can be derived by double application of the rotation matrix $\mathbf{R} = \frac{1}{|\mathbf{u}|}\begin{pmatrix} u_x & u_y \\ -u_y & u_x \end{pmatrix}$ on the diagonal matrix $\mathbf{D}_{diag} = \begin{pmatrix} \alpha_L & 0 \\ 0 & \alpha_T \end{pmatrix}$ (see Zimmerman &

Homsy [vii], Coutinho & Alves [viii], Petitjeans *et al*. [ix]):

$$\mathbf{D} = \mathbf{R}^T \cdot \mathbf{D}_{diag} \cdot \mathbf{R} \qquad (4)$$

The system of equations (1) and (2) is mostly simplified to a system of two differential equations. This can be achieved in several manners. One way is to replace **u** in the first equation of (1) by the explicit formulation of the second equation:

$$\nabla \bullet \frac{\mathbf{k}}{\mu} \nabla p = 0 \qquad (5)$$

With equation (5) an elliptic equation for dynamic pressure $p$ as independent variable results. Alternatively the streamfunction $\Psi$ can be introduced, which is defined by the equations:

$$\frac{\partial \Psi}{\partial x} = u_y \qquad \frac{\partial \Psi}{\partial y} = -u_x \qquad (6)$$

For the streamfunction an elliptical differential equation results, too:

$$\nabla \bullet \frac{\mu}{\mathbf{k}} \nabla \Psi = 0 \qquad (7)$$

which can be verified easily by using equations (1) and (5), utilizing that the partial derivatives in $x$ and $y$ direction for $p$ can be exchanged.

In this model viscosity is concentration dependent. It decreases exponentially with concentration $c$. Following Coutinho & Alves [viii] we assume isotropy of the scalar permeability $k$ and the ratio $\mu/k$ fulfilling the equation

$$\mu / k = \exp(-Rc) \qquad (8)$$

where $R$ is connected with the mobility ratio $M$

$$M = \mu_1 / \mu_2 \qquad (9)$$

by the equation

$$R = \exp(M) \qquad (10)$$

$\mu_1$ is the viscosity of the replacing fluid, and $\mu_2$ the viscosity of the replaced fluid.

In some publications another formulation of the partial differential for the streamfunction $\Psi$ is used. In analogy to Zimmerman & Homsy [vii] using the Langrangian formulation, Chen & Wang [x] denote the streamfunction equation as:

$$\nabla^2 \Psi = -R \nabla \Psi \bullet \nabla c \qquad (11)$$

Equation (11) is equivalent to equation (7), but is more complex and more difficult to solve. For that reason in our numerical simulations we prefer the formulation given before.

There is another instance in which the presented model differs from those presented by the authors cited above. Zimmerman & Homsy [vii], and Ghesmat & Azaiez [xi] transfer the problem to a moving coordinate system. For the Lagrangian system they obtain a modified differential equation and also different boundary conditions. Similar transformations are utilized by de Wit *et al.* [xii], and Mishra *et al*. [xiii].

Coutinho & Alves [viii] report about numerical modelling in the Eulerian system, which we also use in this paper. In contrast to the latter authors, who use the pressure formulation, we prefer the streamfunction for the flow equation. We like streamlines to be obtained directly as contour lines for $\Psi$. Another difference concerns the boundary conditions: the model region of Coutinho & Alves [viii] is closed and they use sink and source terms to simulate the flow regime.

## 3. Model Region, Boundary Conditions and Parameters

The model region is a strip of 500 m length ($x$-direction) and 125 m width ($y$-direction). A less viscous fluid is entering on the left, and flowing between two impermeable horizontal boundaries towards the outlet, gradually replacing the highly viscous fluid that is present initially.

The situation is realized by implementing boundary conditions as follows. There is inflow at $x$=0 boundary with the Neumann condition $\partial \Psi / \partial x = 0$ for the streamfunction and Dirichlet condition $c$=1 for the concentration. At the outflow boundary $x$=$L$ there are Neumann conditions for both streamfunction and concentration: $\partial \Psi / \partial x = 0$ and $\partial c / \partial x = 0$, respectively. At the horizontal boundaries we require Dirichlet conditions for the streamfunctions: $\Psi = \Psi_0$ at the lower ($y$=0) boundary and $\Psi = 0$ at the upper ($y$=$H$) boundary. At these closed boundaries we have the Neumann condition for $c$, which implies that there is no diffusive flux across the boundary.

Due to the vanishing normal velocity component there is also no advective flux.
As initial condition we chose a linear profile for the streamfunction $\Psi = \Psi_0 - y$, which fulfills the boundary conditions. For the concentration we require the condition:

$$c(t=0) = \begin{cases} \xi f(x,y)\exp(-x^2/\sigma^2) & \text{for } x < L/128 \\ 0 & \text{else} \end{cases} \quad (12)$$

The function *f* describes a random disturbance of the initial concentration pattern. $\zeta$ denotes the size of the disturbances and σ the variance in *x*-direction. The disturbed concentration pattern is applid only in the vicinity of the inflow boundary. With these settings we follow Zimmerman & Homsy [vii] as well as Coutinho & Alves [viii], although negative values of concentrations may appear at some locations. However these unrealistic values vanish after a short initial simulation time and can thus not be seen as crucial for the simulation.
All input parameters are listed in Table 1.

**Table 1:** Parameters

| Parameter | Symbol | Value & Unit |
|---|---|---|
| Length | $L$ | 500 m |
| Height | $H$ | 125 m |
| Porosity | $\varphi$ | 1 |
| Max. size of disturbance | $\zeta$ | 0.01 |
| Penetration length | $\sigma$ | 500 m |
| Transversal dispersivity | $\alpha_T$ | 0.05 m |
| Mobility ratio | $M$ | log(3) |

## 4. Use of COMSOL Multiphysics

For the simulations we used COMSOL Multiphysics software, which is based on the Finite Element method. Following the multiphysics concept of the software, we use two coupled 'application modes'. Each of the two modes (Poisson, convection-diffusion) corresponds to a physical process or phenomenon (fluid flow, solute transport), and to a differential equation (equations (7) and (2)). The transport mode is linked to the flow mode, as the velocities, which are processed from the streamfunction according to equations (6), are required. The velocity components appear in the advective term as well as in the dispersion term (see equation (3)). The flow mode is linked to transport, as the viscosity/permeability ratio as parameter is concentration dependent, according to formula (8). The system of differential equation is coupled by these feedbacks.
Note that one of the two equations is steady-state (flow), while the other is transient (transport). Altogether the coupled system is transient. Physically speaking the response of the flow to changes of the solute distribution is so fast that a corresponding storage term is neglected in equation (7) (as also already in equations, (5) and (1)).
In the model longitudinal dispersivity $\alpha_L$ is connected to transversal dispersivity $\alpha_T$ by:

$$\alpha_L = 1 + \alpha_T\left(1 - u_x^2 - u_y^2\right) \quad (13)$$

(see also Coutinho & Alves [viii]). We did not apply any artificial diffusion option. These options may be used to stabilize the numerical algorithm. However, the results may differ significantly from the physical solution, if numerical diffusion exceeds real diffusivities or dispersivities.
The initial state for the concentration distribution is implemented as a MATLAB@ function, following equation (12).

**Table 2:** Execution time with different meshes

| Mesh, # elements, DOFs | | Type | Execution time (s) (version 3.5a) |
|---|---|---|---|
| 156 | 702 | free | 1.4 |
| 354 | 2650 | " | 5.2 |
| 2496 | 10290 | " | 35.3 |
| 9984 | 40546 | " | 320.8 |
| 16384 | 132354 | mapped | 721.7 |

The equations are discretized according to the method of Finite Elements. We use quadratic Lagrange elements for both variables. Table 2 provides an overview how execution time depends on meshes, free or mapped.
The comparison of the runs with the finest free mesh and the mapped mesh indicates that models with mapped mesh perform faster than free mesh models of the same size. While the mapped mesh has more than three times more DOF, its execution time exceeds that of the free mesh run only by a factor slightly above 2. However for coarse mapped meshes the numerical results become completely wrong; for details see next section.

**Table 3:** Performance of linear solvers

| **Solver** | **Execution time (s)** | |
|---|---|---|
| | **COMSOL version 3.4** | **COMSOL version3.5a** |
| UMFPACK | 153.3 | 131.7 |
| SPOOLES | 204.7 | 178.1 |
| PARDISO | 135.4 | 67.2 |
| PARDISO (out of core) | - | 187.7 |
| GMRES | 221.5 | 107.4 |
| FGMRES | 293.2 | 76.9 |
| Conjugate gradient | no convergence | no convergence |
| BICGSTAB | - | 81.1 |
| Multigrid | no convergence | no convergence |

Flow and transport modes are solved simultaneously for the model. The resulting non-linear system is solved by the Newton method, solving a linear system in each iteration step. First we explored the performance of several linear solvers, without changing any other parameters from their default values (we set relative accuracy to 0.01, and absolute accuracy to 0.001) for the free mesh model. The outcome of the solver test is given in Table 3. Obviously the PARDISO solver performs best. For that reason we investigated the effect of various options of the PARDISO solver. Shortest execution time of about 104 s (version 3.4) and 39.9 s (version 3.5a) for the reference set-up was obtained by using the 'minimum degree option' (instead of 'nested dissection'), 'automatic' check of tolerances (instead of 'on' or 'off') and disabled row pre-ordering.

## 5. Results

First results with coarse meshes show that the results depend very much on the mesh size. The models with mapped meshes (128 x 32, 120 x 40) did not lead to fingering. The mesh with 128 x 64 rectangular elements, corresponding to 66306 DOF (execution time: 822 s), as well the mesh with 256 x 64 elements (132354 DOF, execution time: 1593 s), led to fingering!
The model reported in the following has 15744 elements with quadratic basis functions, which corresponds to 8025 mesh points and 63586 DOF (degrees of freedom). It is based on a free mesh with minimum quality of the elements of 0.756 and the element area ratio of 0.238.
Figure 1 shows the development of viscous fingering. The concentration is depicted as surface plot, where the dark color represents the replaced and the light color the replacing fluid. The transition zone between these fluids is very narrow.
It is clearly visible that small fingers appear in the transition zone between the two phases a short time after the start of the simulation. While the front, which is not a straight line anymore, is penetrating from the left, the fingers grow in size. In the final figure ($T$=300) we observe the merging of the last remaining two fingers.
Also shown in the plots are the streamlines, which are obtained here as contour lines of the streamfunction (they could also be constructed by using 'streamline' from the COMSOL post-processing mode).
In addition we visualize the flow field by an arrow field, representing velocities. The figures show the effects on the flow field. The quasi-1D initial and mean state is disturbed significantly with the penetration of the entering fluid. In the transition zones there are steep velocity gradients in $y$-direction. In the last two figures it becomes very obvious that the flow in the replacing fluid is much faster than in the initial fluid, where the velocities have become very low.

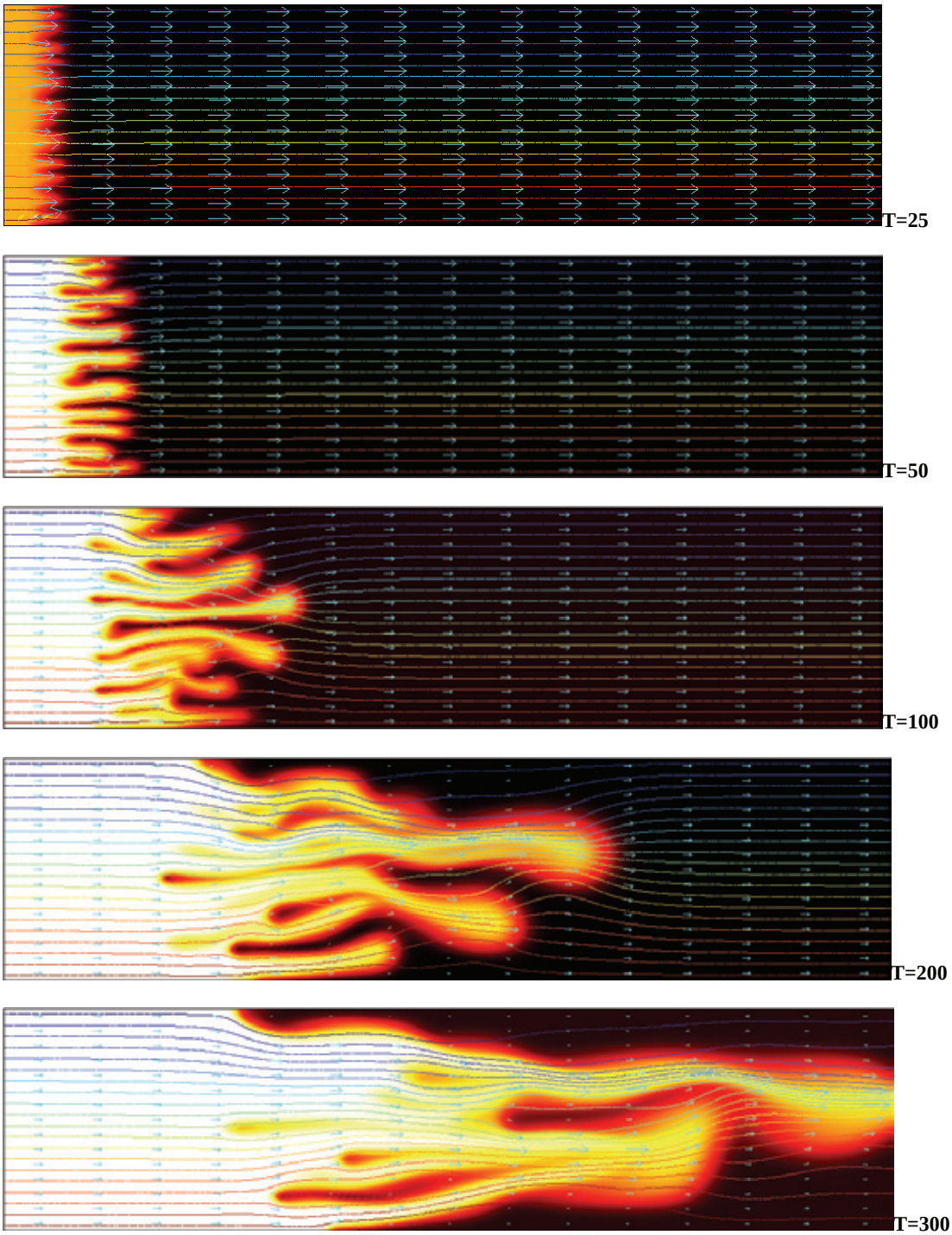


**Figure 1**: Finger development, depicted for different time instants $T$ by concentration $c$ as surface plot, streamlines and velocity distribution, represented by an arrow field

## 6. Conclusions

Fingering phenomena can be modeled well by COMSOL Multiphysics.

Comparison with results obtained by other modelers shows that the fingering dynamics is well captured, although finger details are quite different. This is not astonishing as the details of the fingers depend among other circumstances also on the random field, used as an initial condition for *c*. The random fields differ depending on the random number generators used by different modelers. Moreover the random field is also different for the different meshes; and thus fingering details can expected to differ even for the same model and parameters, if only a different mesh is used.

## 7. References


i Brailovsky I, Babchin A, Frankel M, Sivashinsky G., Fingering instability in water-oil displacement, *Transport in Porous Media* **63**, 363-380 (2006)

ii Garcia JE, Pruess K, Flow instabilities during injection of $CO_2$ into saline aquifers, TOUGH Symp., Proc. (2003)

iii Zhang ZF, Smith JS Visualization of DNAPL fingering processes and mechanisms in water-saturated porous media, *Transport in Porous Media* **48**, 41-59 (2002)

iv Perugini D, Poli G, Rocchi S, Development of viscous fingering between mafic and felsic magmas: evidence from the Terra Nova Intrusive Complex (Antarctica), *Mineralogy and Pertology* **83**, 1551-166 (2005)

v Zitha PJ, Nguyen QP, Currie PK, Buijse MA, Coupling of foam drainage and viscous fingering in porous media revealed by X-ray computed tomography, *Transport in Porous Media* **64**, 301-313 (2006)

vi Saffman PG, Taylor GI, The penetration of a fluid into a porous medium or Hele-Shaw cell containing a more viscous fluid, *Proc. Royal Soc. London* **A24**, 312-329 (1958)

vii Zimmerman WB, Homsy GM, Nonlinear viscous fingering in miscible displacements with anisotropic displacements. *Phys. Fluids* **A 3**, 1859-72 (1991)

viii Coutinho ALGA, Alves JLD, Finite element simulation of nonlinear viscous fingering in miscible displacements with anisotropic dispersion and nonmonotonic viscosity profiles. *Comp. Mech*. **23**, 108-116 (1999)

ix Petitjeans P, Chen CY, Meiburg E, Maxworthy T, Miscible quarter five-spot displacements in a Hele-Shaw cell and the role of flow-induced dispersion. *Physics of Fluids* **11**(7), 1705-1716 (1999)

x Chen CY, Wang SW, Miscible displacement of a layer with finite width in porous media. *Int. J. Num. Meth. for Heat & Fluid Fluid Flow* **11**(8), 761-778 (2001)

xi Ghesmat K, Azaiez J, Viscous fingering instability in porous media: effect of anisotropic velocity-dependent dispersion tensor, *Transport in Porous Media* **73**, 297-318 (2008)

xii de Wit A, Bertho Y, Martin M, Viscous fingering of miscible slices, *Phys. Fluids* **17**(5), 054114-054114-9 (2005)

xiii Mishra M, Martin M, de Wit A, Differences in miscible viscous fingering of finite width slices with positive or negative log-mobility ratio, *Phys. Review* **E 78**, 066306-1-11 (2008)